J Physiol 587.20 (2009) pp 4769–4783

The Journal of Physiology

The response of the tandem pore potassium channel TASK-3 (K_{2P}9.1) to voltage: gating at the cytoplasmic mouth

I. Ashmole[1], D. V. Vavoulis[2], P. J. Stansfeld[3], Puja R. Mehta[1], J. F. Feng[2], M. J. Sutcliffe[4] and P. R. Stanfield[1]

Departments of [1]Biological Sciences and [2]Computer Science, University of Warwick, Coventry CV4 7AL, UK
[3]Structural Bioinformatics and Computational Biochemistry Unit, Department of Biochemistry, University of Oxford, South Parks Road, Oxford OX1 3QU, UK
[4]Manchester Interdisciplinary Biocentre and School of Chemical Engineering and Analytical Science, University of Manchester, 131 Princess Street, Manchester M1 7DN, UK

Although the tandem pore potassium channel TASK-3 is thought to open and shut at its selectivity filter in response to changes of extracellular pH, it is currently unknown whether the channel also shows gating at its inner, cytoplasmic mouth through movements of membrane helices M2 and M4. We used two electrode voltage clamp and single channel recording to show that TASK-3 responds to voltage in a way that reveals such gating. In wild-type channels, P_{open} was very low at negative voltages, but increased with depolarisation. The effect of voltage was relatively weak and the gating charge small, ∼0.17. Mutants A237T (in M4) and N133A (in M2) increased P_{open} at a given voltage, increasing mean open time and the number of openings per burst. In addition, the relationship between P_{open} and voltage was shifted to less positive voltages. Mutation of putative hinge glycines (G117A, G231A), residues that are conserved throughout the tandem pore channel family, reduced P_{open} at a given voltage, shifting the relationship with voltage to a more positive potential range. None of these mutants substantially affected the response of the channel to extracellular acidification. We have used the results from single channel recording to develop a simple kinetic model to show how gating occurs through two classes of conformation change, with two routes out of the open state, as expected if gating occurs both at the selectivity filter and at its cytoplasmic mouth.

(Received 14 May 2009; accepted after revision 24 August 2009; first published online 24 August 2009)
Corresponding author P. R. Stanfield: Department of Biological Sciences, University of Warwick, Coventry CV4 7AL, UK. Email: p.r.stanfield@warwick.ac.uk

Introduction

Tandem pore potassium channels help set the resting membrane potential of a wide variety of cells (Goldstein *et al.* 2001; Patel & Honoré, 2001; Kim, 2005). Among such channels, the acid sensitive TASK-3 (K_{2P}9.1) is widely expressed in the central nervous system, regulating the excitability of a number of neuronal populations (e.g. Han *et al.* 2002, 2003; Washburn *et al.* 2002; Brickley *et al.* 2007). And in the adrenal cortex, the channel plays a crucial role in the regulation of aldosterone secretion from the zona glomerulosa (Czirják *et al.* 2000; Czirják & Enyedi, 2002).

Channels of the TASK subfamily are shut by extracellular acidification (Duprat *et al.* 1997; Kim *et al.* 1998; Leonoudakis *et al.* 1998; Kim *et al.* 2000; Rajan *et al.* 2000). Protonation of the side chain of a histidine residue, H98, located in the outer mouth of the channel (Kim *et al.* 2000; Rajan *et al.* 2000; Lopes *et al.* 2001; Ashmole *et al.* 2001; Morton *et al.* 2003) initiates a conformation change that results in channel closure (Yuill *et al.* 2007; Stansfeld *et al.* 2008). This gating process, occurring at the selectivity filter, is likely to be similar to that described for C-type inactivation in Kv channels (Yellen, 1998; Bichet *et al.* 2003; see also Zilberberg *et al.* 2001).

There is currently little or no evidence that mammalian TASK channels are gated at the inner, cytoplasmic mouth. Such channels are, however, modulated by a number of factors. For example, depolarisation of the membrane gates TASK channels open (Lopes *et al.* 2000; Yuill *et al.* 2007), though the effect of voltage is weak compared with that on channels of the voltage gated superfamily. Further, while TASK channels are down-regulated by Gq coupled receptors (Millar *et al.* 2000; Czirják *et al.* 2000; Talley *et al.* 2000), channel opening is promoted by volatile anaesthetics such as halothane (Talley & Bayliss, 2002). The responses to Gαq on the one hand and

DOI: 10.1113/jphysiol.2009.175430

to halothane on the other occur independently of the response to extracellular acidification (Talley & Bayliss, 2002), implying that a further gating mechanism occurs.

Studies of bacterial K^+ channels in shut (KcsA, KirBac1.1; Doyle *et al.* 1998; Kuo *et al.* 2003) and in open form (MthK, Jiang *et al.* 2002) show gating to involve straightening and flexion of membrane helices about a glycine hinge residue. Such glycine hinge residues are conserved in the M2 and M4 membrane helices of all tandem pore K^+ channels. This conservation suggests that similar gating changes occur in these channels and may be the mechanism through which TASK channels respond to Gq coupled receptors, to volatile anaesthetics, and to voltage.

Here, we consider the response of TASK-3 channels to voltage as a means of investigating channel gating. We find residues in M2 and M4 whose mutation increases channel open state probability. We also find that mutation of putative hinge glycines (G117 and G231), preventing easy flexion of M2 and M4, holds channels shut. All of these mutant channels show an alteration in the relationship between P_{open} and voltage, though the apparent gating charge is not altered. None of the mutants showed markedly altered sensitivity to changes in extracellular pH. Our results are consistent with channel gating occurring at the channel inner mouth, through movements of M2 and M4.

Since it is proposed that channels are opened and shut both at the selectivity filter (Yuill *et al.* 2007) and at the cytoplasmic mouth, we have used the results of single channel recording to develop a simple kinetic model to test whether the hypothesis of two modes of gating can account for our results (see Discussion). A model with two routes from the open to different shut states accounts well for our results.

Some of the results have been described in abstract form (Stanfield *et al.* 2008). A similar conclusion has recently been reached by Ben-Abu *et al.* (2009) for the *Drosophila* channel KCNK0, which, however, is constitutively open and whose P_{open} is independent of voltage.

Methods

Molecular biology

The human TASK-3 cDNA was cloned by PCR using as template first strand cDNA reverse transcribed from total RNA purified from CAPAN-1 cells (a cell line derived from a pancreatic duct carcinoma; Fanjul & Hollande, 1993). CAPAN-1 cells were purchased from American Type Culture Collection (ATCC). The resulting product was cloned into the mammalian expression vector pcDNA3 and the entire open reading frame sequenced. For expression in *Xenopus* oocytes the TASK-3 cDNA was sub-cloned as a *Bam*H1 fragment into the vector pBF. Mutants were generated by the QuikChange method (Stratagene, La Jolla, CA, USA) and were verified by sequencing of the entire mutant cDNAs.

Electrophysiology: two electrode voltage clamp

Complementary RNAs (cRNAs) were synthesised *in vitro* from *Mlu*I-linearised pBF vector, using SP6 polymerase (Ambion, Inc., Austin, TX, USA). Electrophysiological recordings were carried out on TASK-3 channels expressed in oocytes obtained from *Xenopus* frogs anaesthetised by immersion in 0.3% (w/v) MS222 and killed by destruction of the brain and spinal cord. Oocytes were injected with up to 50 ng cRNA and recordings were made 1–3 days after injection. Water injected oocytes were used as control in previous experiments (Yuill *et al.* 2007) and native currents were consistently too small to interfere materially with those recorded from TASK channels.

Membrane currents were recorded with a two-electrode voltage clamp using a GeneClamp 500B amplifier, a Digidata 1322A interface and pCLAMP version 10.1 software (all Axon Instruments, Union City, CA). Currents were filtered at 2 kHz and digitised at 10 kHz. Experiments were carried out at room temperature (~20°C). Some experiments used a low K^+ solution containing (mmol l^{-1}): 4 KCl, 92 *N*-methyl-D-glucamine (NMDG), 1 $CaCl_2$, 1 $MgCl_2$, 10 *N*-2-hydroxyethylpiperazine-N′-2-ethanesulphonic acid (Hepes), pH adjusted to 7.5 using HCl. A low K^+ solution at pH 5.0 was also used, buffered with 2-(*N*-morpholino)ethanesulphonic acid (Mes) at 10 mmol l^{-1}. Experiments testing the response to changes of extracellular pH used high K^+ solutions, containing (mmol l^{-1}): 70 KCl, 26 *N*-methyl-D-glucamine, 1 $CaCl_2$, 1 $MgCl_2$, 10 Hepes, pH adjusted using HCl. To test pH sensitivity, we used 10 mM Hepes for solutions at pH 7.0 to 8.0, piperazine-1,4-bis-2-ethanesulphonic acid (Pipes) for pH_o 6.5, and Mes for pH_o 5.0 and 6.0. In some experiments 10 mM trishydroxymethylaminomethane was used at pH 8.0 and 10 mM Pipes at pH 7.0. The fitting of the time course of currents was done using the pCLAMP fitting routines; the fitting of other experimental results used SigmaPlot, v. 9.0 (Systat Software Inc., San Jose, CA, USA).

Electrophysiology: single channel recording

Chinese hamster ovary cells (CHO-K1, ATCC) were cultured in Ham's F12 medium (Invitrogen) supplemented with 10% (v/v) fetal calf serum. Cells were co-transfected with wild-type or mutant TASK-3 cDNAs in pcDNA3 and with a plasmid directing the expression of enhanced green fluorescent protein (EGFP) as a transfection marker. Lipofectamine LTX transfection reagent

(Invitrogen) was used according to the manufacturer's instructions.

For single channel recording, an Axopatch 200A amplifier, Digidata 1322A interface and pCLAMP version 9.02 software were used. Patch pipettes were pulled from thick walled glass (Harvard Apparatus, Holliston, MA, USA) and coated with Sylgard. The pipette solution contained (mmol l^{-1}): 2 $CaCl_2$, 10 Hepes titrated to pH 7.2 with KOH plus KCl to bring $[K^+]$ to 140 mmol l^{-1}. The bath solution contained $MgCl_2$ at 2 mmol l^{-1} in place of $CaCl_2$, and ethylene glycol-bis(2-aminoethylether)-*N*,*N*,*N*′,*N*′-tetra-acetic acid (EGTA) at 5 mmol l^{-1}. Recordings were made at room temperature (∼20°C) from excised, inside-out membrane patches by filtering at 2 kHz (−3 dB, 4-pole Bessel) and digitising at 10 kHz.

Data analysis used the trace analysis (TRACAN) software, written and generously provided by Dr N. W. Davies (Department of Cell Physiology and Pharmacology, University of Leicester). Channel amplitudes were determined by fitting an amplitude histogram of data points. Open and shut durations were determined in single channel patches using a cursor set mid way between the shut and open levels. In fitting such relationships, given the filter setting and digitisation rates, a minimum resolution of 100 μs was applied (Colquhoun & Sigworth, 1995). No correction was applied for missed events owing to the small reduction in dwell times (∼5%) that resulted from such correction. The distributions of dwell times in open and shut states were fitted with appropriate exponential functions. The distribution of the number of openings per burst was fitted with the geometrical distribution given by Colquhoun & Sigworth (1995), where the probability $P(r)$ of seeing r openings in a given burst is:

$$P(r) = (1 - \rho)\rho^{r-1}. \quad (1)$$

As r increases, $P(r)$ decreases by a step factor ρ, here computed from the observed mean number (μ) of openings per burst by the expression: $\mu = (1 - \rho)^{-1}$.

In multichannel patches, P_{open} was computed by measuring occupancy of different levels of current, with 0, 1, 2, etc. channels open and evaluating $\sum_{j=1}^{N} t_j j / TN$, where t_j is the time spent at level j in a patch containing N active channels, with a duration of recording T. N was chosen as the maximum number of channels seen at positive voltages during the period of recording (≥20 s). Since P_{open} was low in some cases, the estimate for N is likely to be a lower limit, and the values given for P_{open} will be an upper limit.

Results are given as mean ± S.E.M. Where appropriate, ANOVA was used to test for significance of difference.

Kinetic modelling

A four-state kinetic model of TASK-3 with three shut and one open states (see Discussion, Scheme 1) was constructed and fitted against data derived from the analysis of single channel recordings from wild and mutant types.

The backward and forward transition rates between any two different states were modelled as exponential functions of membrane potential of the form found in Eyring barrier models. Various measured quantities – the distribution of open and brief shut dwell times, the number of openings per burst and the open probability – were calculated as functions of these transition rates (Colquhoun & Hawkes, 1995) and then simultaneously fitted against single-channel experimental data, using a non-linear least squares algorithm implemented in the function *lsqcurvefit* from the MATLAB (The Mathworks, Inc., Natick, MA, USA) Optimization Toolbox. The fitting was first done against data from wild-type channels and repeated for data from a mutant channel type (A237T). The fitting was based on a three-state subset of the four-state model (formed by state 1, state 2 and state 3; see Scheme 1), which was sufficient for estimating the complete set of transition rates that appear in the four-state model.

Computational chemistry and molecular modelling

We have previously built models of TASK-1 in putative shut and open states (Yuill *et al.* 2007). Here, a homology model of TASK-3 (SWISS-PROT ID: Q3LS21; Boeckmann *et al.* 2003) was created, using Modeller 7v7, based on the pore domain of the KvAP crystal structure (PDB ID: 1ORQ; Jiang *et al.* 2003). The P1 and P2 segments of TASK-3 were treated as separate entities and modelled onto individual subunits of KvAP. In this modelling of P1 and P2, we considered residues only from the N-terminal ends of the pore helixes through to the C-terminal ends of the inner helices (M2 and M4, respectively). Thus P1 was modelled from Phe80 to Phe135 and P2 from Phe186 to Thr251, with twofold symmetry restraints applied to the dimer.

Results

The effect of membrane potential on TASK-3 currents

TASK channels show a weak dependence on voltage. Figure 1*A* shows currents in wild-type TASK-3 recorded from a *Xenopus* oocyte, in 4 mM K^+ solution under two electrode voltage clamp. Leakage and capacity transients have been subtracted so far as possible by taking the difference between currents at pH 7.5 and at pH 5, where channels are shut by protonation. Depolarisation

over a voltage range from −100 mV to +50 mV gave currents which increased substantially with time, reaching a steady state in several milliseconds. Thus the relationship between steady state current and membrane potential shows outward rectification in part because channels open under depolarisation (Fig. 1*C*; see also Fig. 2*B*).

Currents were fitted (Fig. 1*B*) with the expression:

$$I_K = A_1 \exp(-t/\tau_1) + A_2 \exp(-t/\tau_2) + C. \qquad (2)$$

Neither of the time constants showed a marked dependence on voltage (data not shown). The faster (τ_1) of the two time constants had values between 2.3 and 3.8 ms for the currents shown in Fig. 1*A* and *B*. The slower time constant, τ_2, had values in the range 10–17 ms. Similar results were found with three oocytes at pH 7.5 and 5 and with seven oocytes at pH 7 and 5. Similar results have also previously been described for TASK-1 (Yuill *et al.* 2007). Further analysis of voltage dependence used recording of unitary currents and estimates of channel open state probability, P_{open}.

Single channel recording from TASK-3

Figure 2*Aa* and *b* shows records of unitary currents from a patch containing a single TASK-3 channel. The record is characterised by intermittent openings, owing to the very low P_{open} that is characteristic of TASK channels. This low P_{open} appears not to be associated with run down of the channel upon excision of the patch, perhaps owing to depletion of PIP_2 (Chemin *et al.* 2003; Lopes *et al.* 2005), since (i) a low P_{open} was also recorded in on-cell patches, changing little after excision in the inside out mode (tested in 3 patches) and (ii) consistent values were obtained for P_{open} over several minutes of recording.

The unitary current–voltage relationship for TASK-3 shows inward rectification (Fig. 2*B*) and this rectification was associated with a marked increase in noise in the open level (Fig. 2*Ab*). To illustrate the point, the variance of current at the open level (after subtraction of the baseline variance) was increased from 0.104 ± 0.017 pA^2 at −120 mV ($n = 6$) to 0.172 ± 0.028 pA^2 at +120 mV ($n = 6$). The 71% increase is significant ($P = 0.0125$), using a paired t test. In the patches analysed in this way, the current amplitude was 55% smaller at +120 mV,

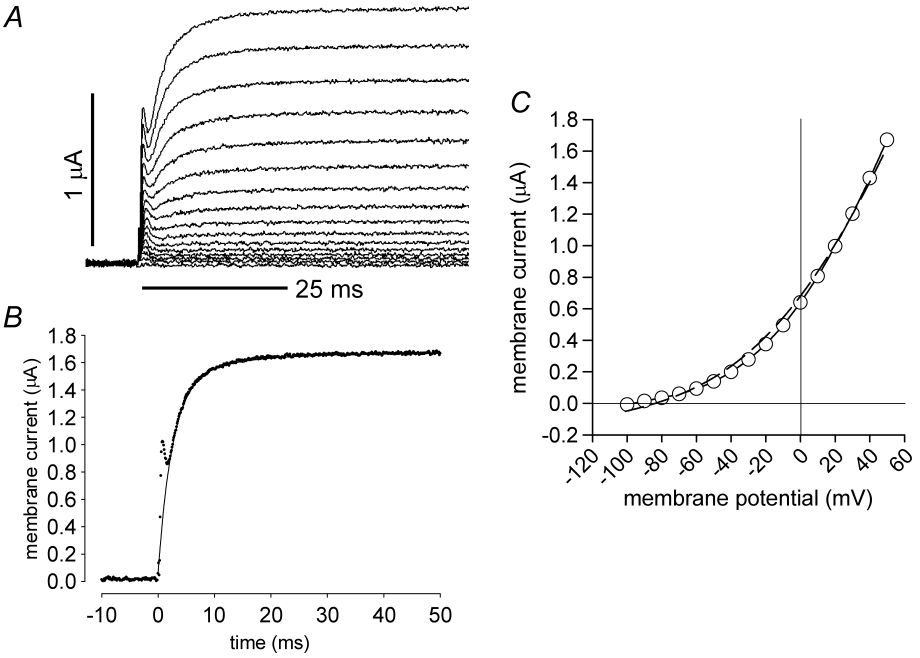

Figure 1. TASK-3 currents show voltage dependence
A, current records obtained from channels expressed in *Xenopus* oocytes under two electrode voltage clamp; these currents were obtained in 4 mM K^+ solution (pH 7.5) with the membrane held at −80 mV, after stepping to −100 mV for 100 ms. Currents are shown for voltage steps from −100 mV, increasing in 10 mV increments to +50 mV. Currents recorded at pH 5.0, when TASK-3 currents were substantially inhibited, have been subtracted. *B*, the Levenberg–Marquardt least squares routine in pCLAMP10 was used to fit current (data points) at +50 mV to the expression: $I = A_1 \exp(-t/\tau_1) + A_2 \exp(-t/\tau_2) + C$. The fit (continuous line) was made between 2.5 and 62.5 ms after the start of the test pulse. At +50 mV, τ_1 was 2.6 ms, while τ_2 was 11.6 ms. A_1, A_2 and C were −1.38, −0.21 and 1.67, respectively. *C*, relationship between steady state current (ordinate) and membrane potential (mV). The continuous line gives a spline curve through the points. The dashed line indicates the fit to constant field theory, where $I_K = P_K \frac{VF^2}{RT} \{ \frac{[K^+]_o \exp(VF/FRT) - [K^+]_i}{\exp(VF/RT) - 1} \}$ with $P_K = 6.38 \times 10^{-8}$ cm^3 s^{-1} and with $[K^+]_i = 115$ mmol l^{-1}. Constant field rectification fits only in the steady state.

compared with −120 mV, a difference that was also significant ($P < 0.001$). Omission of Mg^{2+} from the bath (intracellular face of the patch) solution did not abolish the rectification (data not shown). The unitary conductance of human TASK-3, obtained from the hyperpolarising limb of the current voltage relation, was 18.7 ± 0.7 pS ($n = 17$).

Analysis (Fig. 2*C* and *D*) of the microscopic kinetics gives open times whose distribution fits a single exponential function. The distribution of shut times may be fitted as the sum of two exponential elements, as anticipated from the fit made to macroscopic currents (Fig. 1; eqn (2)). In the single channel patch illustrated, bursts

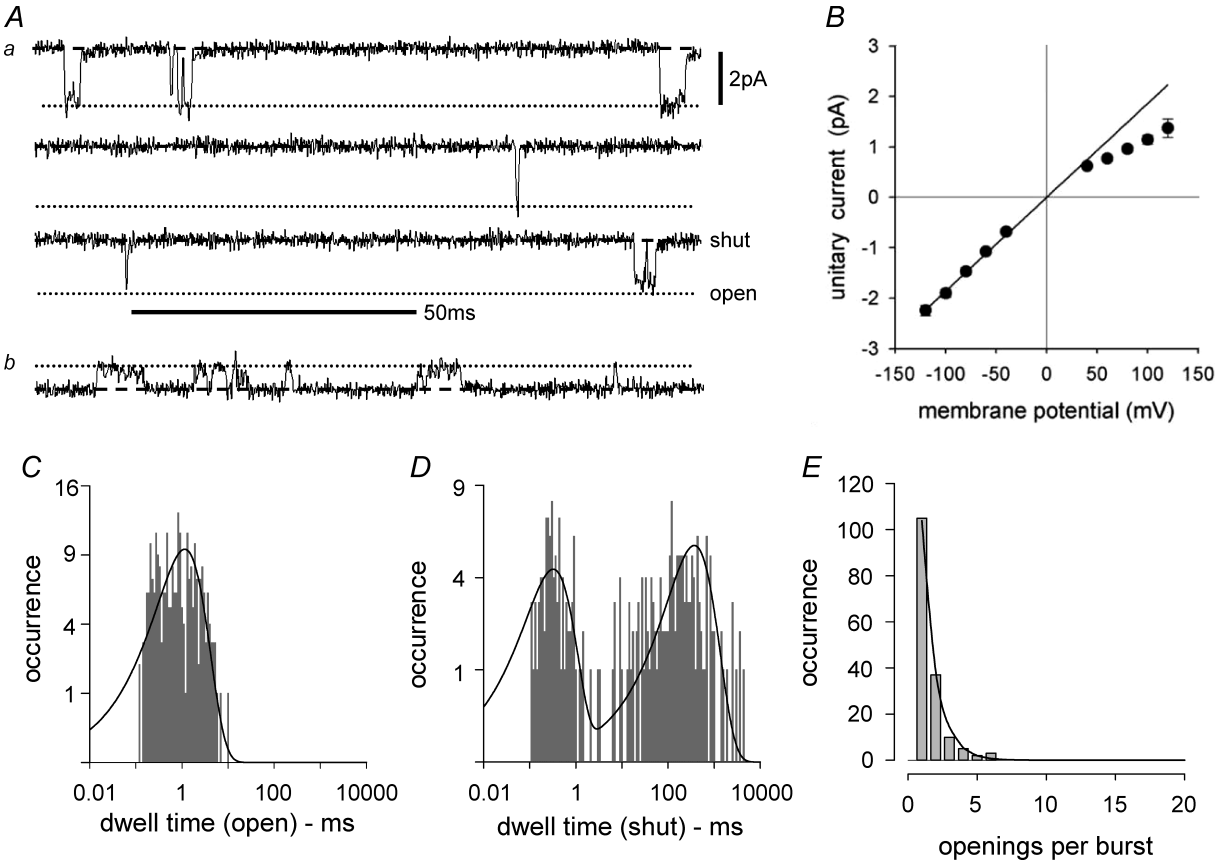

Figure 2. Properties of unitary currents from TASK-3 channels
Aa, unitary currents, obtained from a patch containing a single active channel. Currents were recorded at −120 mV in high K^+ (140 mmol l^{-1}) solution, digitising at 10 kHz (filter, −3 dB at 2 kHz). A long interval between the topmost and the middle record is not illustrated. *Ab*, unitary currents from the same patch at +120 mV, where currents are outward; here the upper level indicates open. *B*, unitary current (ordinate), plotted against voltage (abscissa) for wild-type channels in high K^+ solution. Symbols give mean and error bars ± S.E.M. ($n = 7$–16 patches). The line gives the best fit to the hyperpolarising limb of the current–voltage relationship: outward currents were smaller than predicted from a linear relationship expected with symmetrical K^+ (140 mmol l^{-1}). *C*, distribution of open times for the recording illustrated in *A*, measured using a cursor set midway between open and shut states, with the time for minimum resolution set at 100 μs. The occurrence of dwell times (ordinate; square root scale) is plotted against dwell time in the open state (log scale, abscissa), according to the convention introduced by Sigworth & Sine (1987). The measured values are shown as a histogram in grey. The line gives the best fit, made using a maximum likelihood estimation, with a mean open time of 1.15 ms. 580 openings were detected during the recording. In this patch, open times were 1.58 ms at −100 mV and 1.17 ms at −80 mV. *D*, distribution of shut times: occurrence (ordinate, square root scale) is plotted against the dwell time in shut states (abscissa, log scale). The relationship is fitted with the sum of two exponential components, with time constants of 0.32 and 370 ms. The probability density function for the distribution of shut times is: $pdf_{shut} = 0.14.\exp(-t/0.32) + 207\exp(-t/370)$. *E*, the occurrence of bursts (ordinate) plotted against the number of openings per burst. Bursts were delineated using the criterion of Colquhoun & Sakmann (1985), choosing a critical time (1.72 ms) that equalised the *proportion* of short and of long shut times that were misclassified. Burst durations (not illustrated) were themselves fitted with an expression with two exponential elements, as anticipated from their inclusion of both openings and brief closures. The mean number of openings per burst was 1.59. The number of openings per burst is fitted with the geometric distribution given by eqn (1) in the text (Colquhoun & Sigworth, 1995) and is consistent with a single class of open state.

contain few (1.58) openings at the voltage illustrated (−120 mV), and their distribution is as expected (eqn (1)) if there is one class of open state (Fig. 2*E*). Owing to a marked increase in noise in the open level and the reduced amplitude of outward currents (Fig. 2*Ab*), we used only inward currents to measure dwell times in open and shut states.

Patches containing several channels were also used to measure mean open time and estimate the number of openings per burst. Elements of records were used where openings reached one level only. For all patches analysed, the mean open time for wild-type channels was 1.57 ± 0.17 ms ($n = 6$) at −120 mV, and the number of openings per burst was estimated to be 1.53 ± 0.09 ($n = 6$) at this voltage.

Voltage dependence of P_{open}. The open state probability (P_{open}) of TASK 3 channels increased with depolarisation, as anticipated from the results of two electrode voltage clamp. Figure 3*A* shows this increase recorded in a number of inside-out patches, most of them containing more than one channel. Channel openings appeared to be independent of each other, with the probability of seeing one, two, three, etc. levels of openings being distributed as expected from binomial theorem (data not shown). The increase in P_{open} was fitted with a Boltzmann expression of the form:

$$P_{open} = \left\{1 + \exp\left(\frac{-(V - V')}{k}\right)\right\}^{-1}, \qquad (3)$$

where V' is the voltage at which P_{open} is 0.5 and k is a factor determining steepness. In wild-type channels (Fig. 3*A*), V' is +456 mV and k is 146 mV, suggesting a gating charge (RT/Fk) of 0.17. Such a fit makes a rather severe extrapolation from information from the foot only of the Boltzmann relation. However, the assumptions are not unreasonable since a plot of $\ln(P_{open})$ against membrane potential (Fig. 3*B*) is a line whose slope gives a value of 0.16 for gating charge, little different from that found from the Boltzmann relationship. Further, the relationship that is used to fit the voltage dependence of P_{open} in wild-type channels (Fig. 3*A*) may also be used to fit its voltage dependence in all mutant channels with alteration only in the quantity V' (see below and online Supplemental Material, Supplemental Fig. 1).

The mutant A237T has a raised open state probability. De la Cruz *et al.* (2003) described a gain of function mutation, A237T, in the product of the *sup*-9 gene of *C. elegans*. The product of the *sup*-9 gene is a TASK-channel homologue, and the mutant raised K^+ permeability in muscle, paralysing normal movement. We have made the same mutation (A237T) in the membrane helix M4 of TASK-3 (Fig. 5*A*). (The numbering of residues happens to be the same in the *sup*-9 product and in human TASK-3.)

Single channel recording immediately shows that channel P_{open} is considerably raised at a given voltage from its value in wild-type. Unitary current records from a single channel patch (Fig. 4*A*) show more frequent, longer periods of opening (Fig. 4*C*), grouped into longer bursts (Fig. 4*E*). Unitary currents are larger in A237T (Fig. 4*B*) and the conductance ($\gamma = 22.8 \pm 0.8$ pS; $n = 9$) is significantly higher than in wild-type ($P < 0.01$). As with wild-type, the distribution of open times could be fitted assuming a single type of open state (Fig. 4*C*).

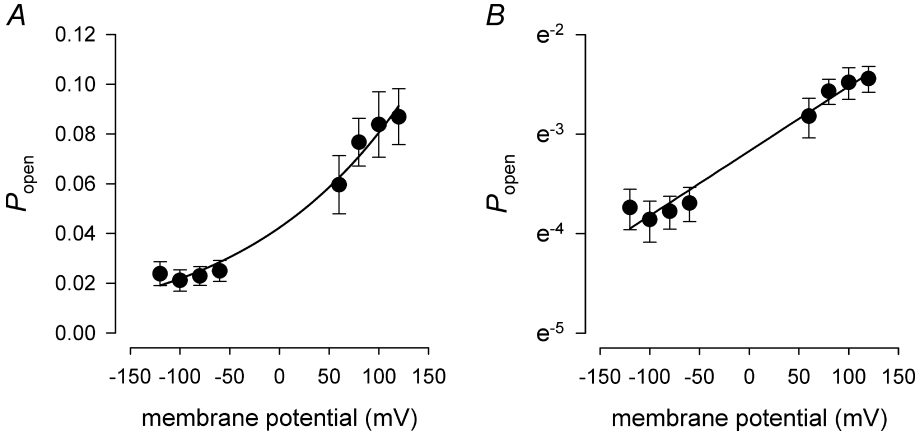

Figure 3. Relationship between P_{open} and membrane potential
A, P_{open} (ordinate) plotted against membrane potential (abscissa). The symbols and error bars give mean ± S.E.M. of measurements from six membrane patches. The line gives the fit to a Boltzmann distribution, $P_{open} = \{1 + \exp(\frac{-(V-V')}{k}\}^{-1}$, with $V' = +456$ mV and $k = 146$ mV (see also eqn (3) in the text). *B*, P_{open} (ordinate, natural log scale) plotted against membrane potential (abscissa). The line fitting the exponential foot of the relationship between P_{open} and membrane potential is drawn according to the expression $P_{open} = P_{open}(0).\exp(V/k)$. $P_{open}(0)$ was 0.042; k was 154 mV. The two methods of fitting (*A* and *B*) gave similar values for the apparent gating charge.

Similarly, shut times are fitted with the sum of two exponential distributions (Fig. 4*D*). While there was an increase in the proportion of short closures, their mean duration was little different from that found in wild-type. Long closures were less frequent and shorter on average in duration (Fig. 4*D*). The occurrence of bursts with different numbers of openings may again be fitted with the geometric distribution used to fit wild-type (eqn (1)), with the mean number of openings per burst raised to 6.27 in the single channel patch illustrated (Fig. 4*E*).

In all patches, including those containing more than one channel, mean open time was 3.80 ± 0.18 ms ($n = 9$) at -120 mV, significantly higher than for wild-type ($P < 0.001$; Fig. 5*E*). The number of openings per burst for all patches with A237T was 4.51 ± 0.34 ($n = 9$) at this voltage, again significantly higher than in wild-type ($P < 0.001$).

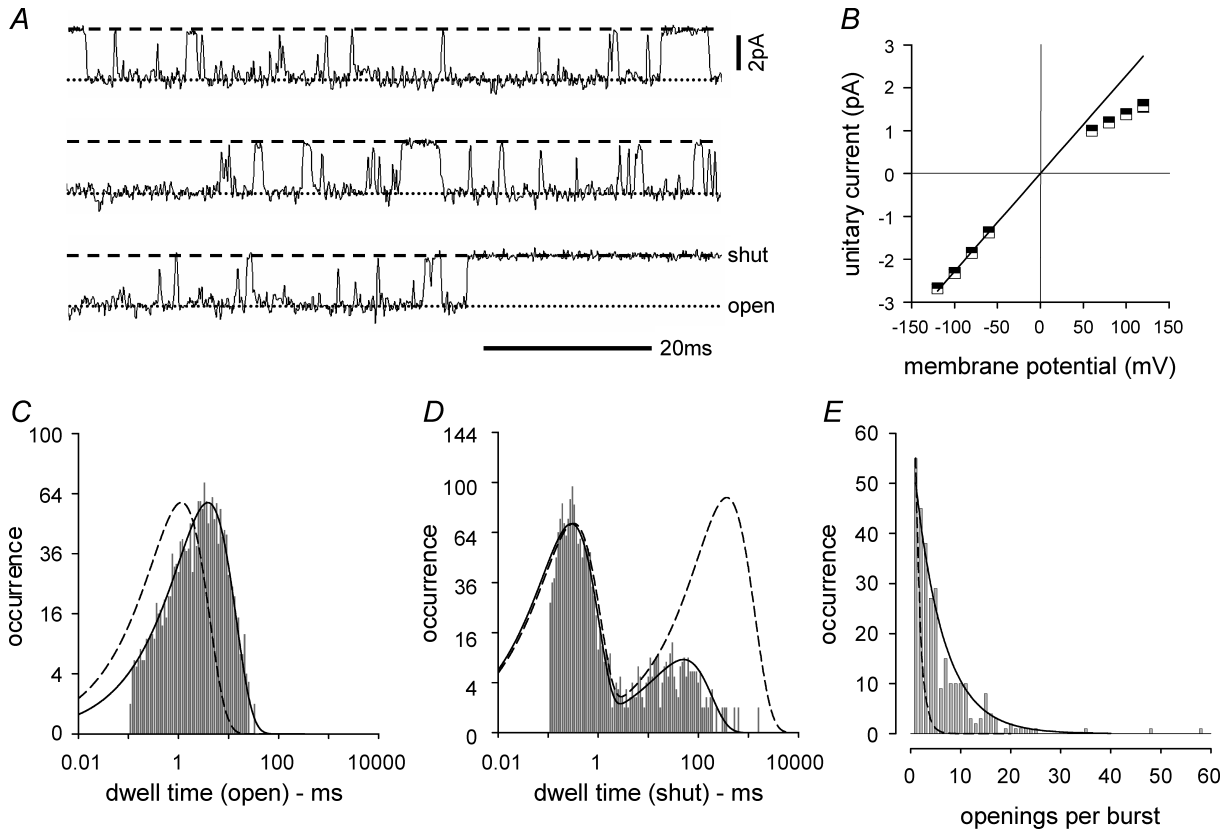

Figure 4. The mutant A237T alters channel microscopic kinetics
A, unitary currents, obtained from a patch apparently containing a single mutant (A237T) channel. Currents are recorded at -120 mV in high K^+ (140 mmol l^{-1}) solution, digitised at 10 kHz (filter, -3 dB at 2 kHz). The three records follow each other without interval. P_{open} was 0.34. *B*, unitary current voltage relationship for recordings from nine patches, with unitary current (pA; ordinate) plotted against membrane potential (mV, abscissa). The semi-filled squares give the mean of the unitary current; in most cases the error bars are smaller than the symbol. *C*, distribution of open times. The occurrence of dwell times (ordinate, square root scale) is plotted against the dwell time in the open state (abscissa, log scale). The bars of the histogram are shown in grey. The continuous line gives the fit with a mean open time of 3.87 ms; the dashed line gives the fit to measurements in wild-type from Fig. 2, scaled to have the same height as the fit for open times in A237T. Open times are longer in A237T. In this patch, open times were 4.49 ms at -100 mV and 4.84 ms at -80 mV. *D*, distribution of shut times: occurrence (ordinate, square root scale) plotted against dwell time in shut states (abscissa, log scale). The relationship is fitted (continuous line) with the sum of two exponential components, with time constants of 0.29 and 50.5 ms. The probability density function for the distribution of shut times is: $pdf_{shut} = 0.26\exp(-t/0.29) + 5.51\exp(-t/50.5)$. The dashed line gives the fit to wild-type (from Fig. 2*D*) scaled to have the same maximum height for the briefer component of closures. The A237T channel visits a long lived shut state less frequently and for a shorter time. *E*, the occurrence of bursts (ordinate) plotted against the number of openings per burst. The mean number of openings per burst was 6.27. As in wild-type, the distribution of burst durations (not illustrated) could be fitted with an expression with two exponential elements owing to the presence of both openings and brief closures. The continuous line in *E* is the fit to a geometric expression (Colquhoun & Sigworth, 1995) assuming a single open state. The dashed line is the fit used for wild-type (Fig. 2), scaled to have the same value when there is only one opening in a burst.

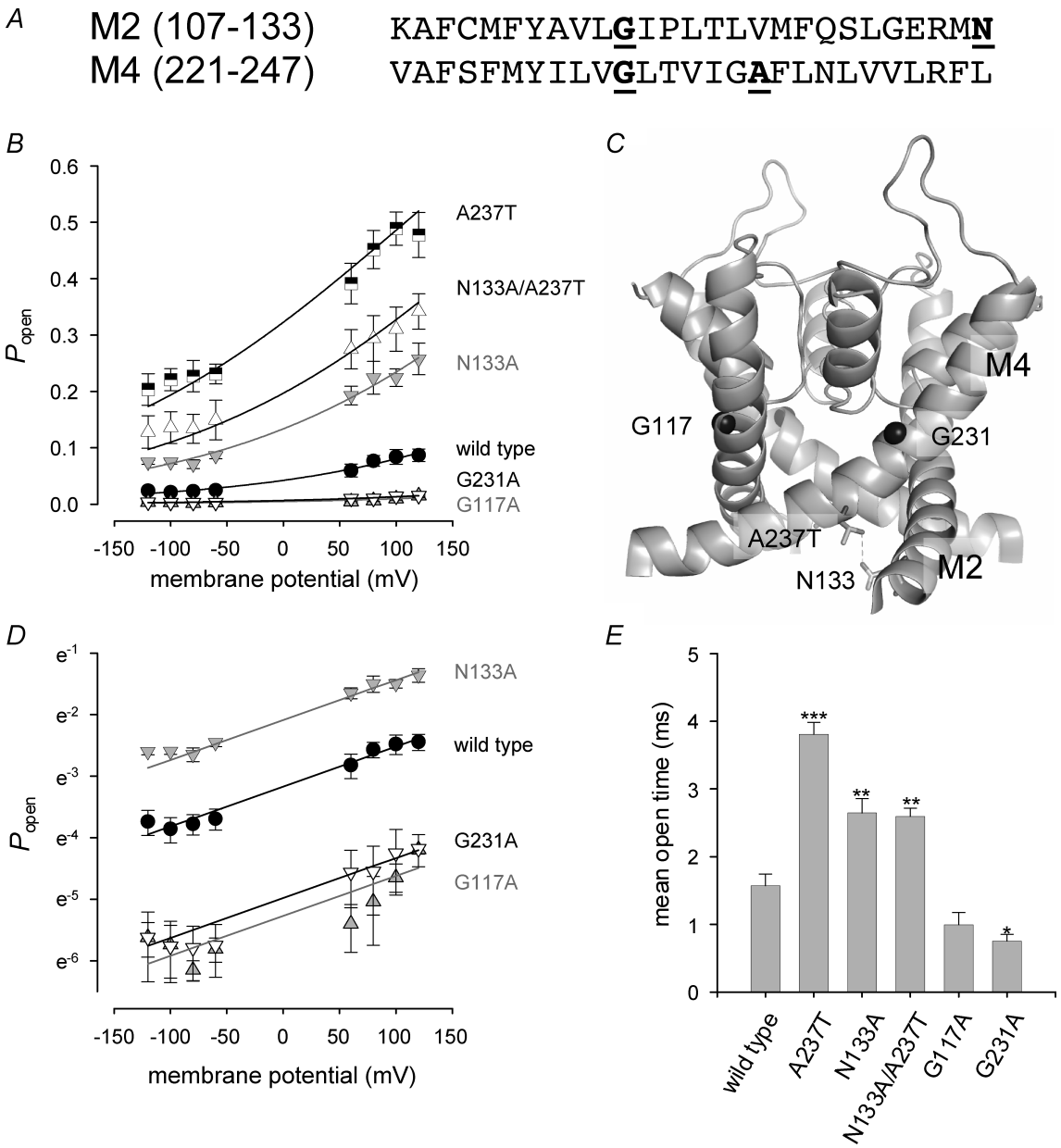

Figure 5. Mutants of M2 and M4 alter P_{open} of TASK-3 channels
A, sequence of M2 and M4 of TASK-3 channels. The positions of A237, N133, G117 and G231 are indicated by underlining. *B*, relationship between P_{open} (ordinate) and membrane potential (abscissa) for mutants A237T (semi-filled squares, mean ± S.E.M., $n = 6$), N133A (grey inverted triangles; $n = 4$), N133A/A237T (open triangles; $n = 5$), G117A (open inverted triangles; $n = 4$) and G231A (grey triangles; $n = 6$). The results for wild-type are given as filled circles. The fits are given by the Boltzmann relation (eqn (3) in the text) used to fit the results from wild-type with only the mid-point of the relationship at V' altered. For gain of function mutants, the relationship is shifted by 344 mV (less positive from its position in wild-type) for A237T, 184 mV less positive for N133A, and 252 mV less positive for the dual mutant N133A/A237T. For loss of function mutants, V' shifted 216 mV *more positive* for G117A and 265 mV more positive for G117A. *C*, structure of a mutant TASK-3 channel modelled in an open state, using the structure of KvAP (Jiang *et al.* 2003) as template. It is hypothesised that channels open through flexion of M2 and M4 around hinge glycines G117 and G231. The positions of these hinge glycines are indicated as spheres in the helices M2 and M4. Gain of function mutants stabilise the open state through altered side chain–side chain interactions between residues. A possible H-bond between Thr in position 237 of M4 (in mutant A237T) and N133, which may contribute to stabilising the open state, is indicated. The model gives a bond length of 3.2 Å. The methyl group of A237 appears to make no hydrophobic contacts with surrounding atoms in a model of the open form of wild-type, which otherwise has an identical conformation to that shown. A model of wild-type TASK-3 in the *shut* state (see Yuill *et al.* 2007 for details of the template used) suggests that, in wild-type,

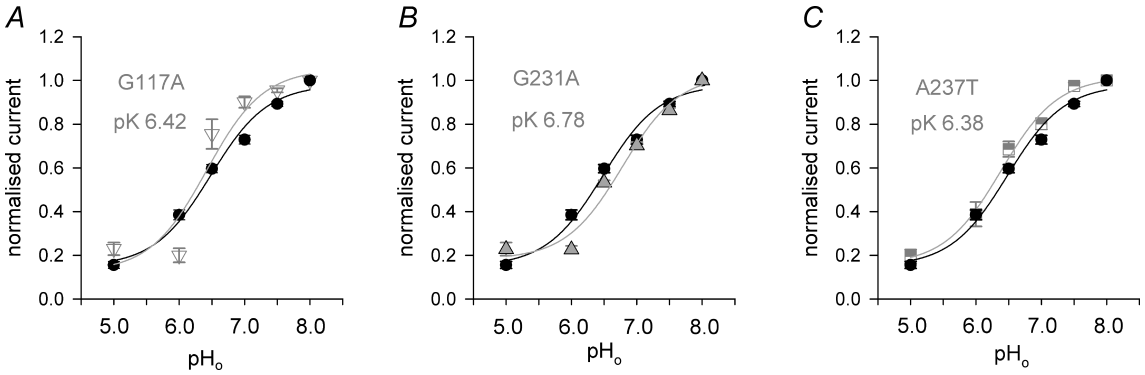

Figure 6. Mutants G117A, G231A and A237T retain pH sensitivity
A, currents recorded from wild-type (filled circles) and G117A mutant channels (inverted triangles), normalised to their values at pH_o 8.0 (ordinate), plotted against extracellular pH (pH_o; abscissa). The error bars indicate ± S.E.M.; results are from 15 oocytes for wild-type and 5 for G117A. The normalised currents (I') are fitted by the expression: $I' = a\{1 + \frac{[H^+]_o}{K_a}\}^{-1} + b$, where a represents the fraction of current affected and b the fraction unaffected by altering pH_o; K_a is the dissociation constant of a protonation reaction. pK_a was 6.46 for wild-type and 6.42 for G117A at the voltage illustrated (−40 mV). Currents were recorded under two electrode voltage clamp after expression of channels in *Xenopus* oocytes. *B*, normalised current (ordinate) plotted against pH_o (abscissa) for wild-type (black circles) and G231A mutant channels (grey triangles). pK was 6.78 for G231A at the voltage illustrated (−40 mV). The results for G231A are from 5 oocytes. *C*, normalised current (ordinate) plotted against pH_o (abscissa) for wild-type (black circles) and A237T mutant channels (semi-filled squares). The recordings in A237T were from 6 oocytes. pK was 6.38 for A237T at the voltage illustrated (−40 mV). Currents recorded through A237T channels were larger than those seen in wild-type, in spite of the reduced amount of cRNA injected to give expression.

Mutants of M2 and M4 that raise P_{open}. For A237T, the relationship between P_{open} and voltage (Fig. 5*B*) was similar to that for wild-type, but was shifted 344 mV to less positive voltages (see also Supplemental Fig. 1). P_{open} was significantly increased over that found for wild-type for a given membrane potential ($P < 0.001$ at each voltage measured). The change in the value of V' in eqn (3) when the channel is mutated from wild-type to A237T is equivalent to a *change* in the energy difference between open and shut states of 5.4 kJ mol^{-1}. The finding argues that different side chain–side chain interactions occur in open and in shut states and is consistent with movement of M4 in the conformation change that occurs upon gating.

A model of TASK-3 in an open state, built using KvAP as template (Fig. 5*C*), assumes channel opening occurring through flexion of M2 and M4 around hinge glycines (G117 and G231). In wild-type, modelling of the open form of the channel suggests that the methyl of the A237 side chain acts as a small space filler, making no obvious hydrophobic contacts with surrounding atoms (not shown). However in the mutant form, an H-bond is predicted between Thr at position 237 and an Asn residue in position 133 (in M2; Fig. 5*A*), contributing to holding the channel open. The putative H-bond is predicted to occur between residues of the adjacent subunits.

However, the mutant N133A (Fig. 5*A*; mutation of M2) also significantly raised both P_{open} ($P < 0.05$ at all positive voltages measured; Fig. 5*B*), and mean open time ($P < 0.01$; Fig. 5*E*). The effect will also reflect altered side chain–side chain interactions, but our modelling currently gives us no insight into the nature of these modified interactions. The dual mutant N133A/A237T raised P_{open} (Fig. 5*B*), but by an amount significantly less than that seen in A237T ($P < 0.05$, except for −120 mV). Mean open time (2.59 ± 0.21 ms at −120 mV, $n = 7$) was also increased significantly over its value in wild-type (Fig. 5*E*), and, in parallel with what is found for P_{open}, the increase was significantly less than

A237 contributes to stabilising the shut state through an interaction with L128 in M2 (not shown). *D*, relationship between lnP_{open} (ordinate) and membrane potential (abscissa) for mutant channels N133A (grey inverted triangles); G117A (grey triangles) and G231A (open inverted triangles, mean ± S.E.M.; $n = 6$). The results are fitted assuming that P_{open} increases exponentially with depolarisation with a gating charge identical with that found for wild-type. A least squares fit to each relationship gave a gating charge of 0.14 for G117A, 0.18 for G231A and 0.15 for N133A, similar to the value of 0.16 found for wild-type (see also Fig. 3*B*). *E*, bar chart illustrating mean open time (ordinate) for channels at −120 mV for wild-type channels ($n = 6$) and for mutants A237T ($n = 9$), N133A ($n = 5$), N133A/A237T ($n = 7$), G117A ($n = 4$) and G231A ($n = 7$). The mutants are indicated on the abscissa. The error bars give ± S.E.M. Significance of difference from wild-type is indicated by *** ($P < 0.001$), ** ($P < 0.01$), or * ($P < 0.05$).

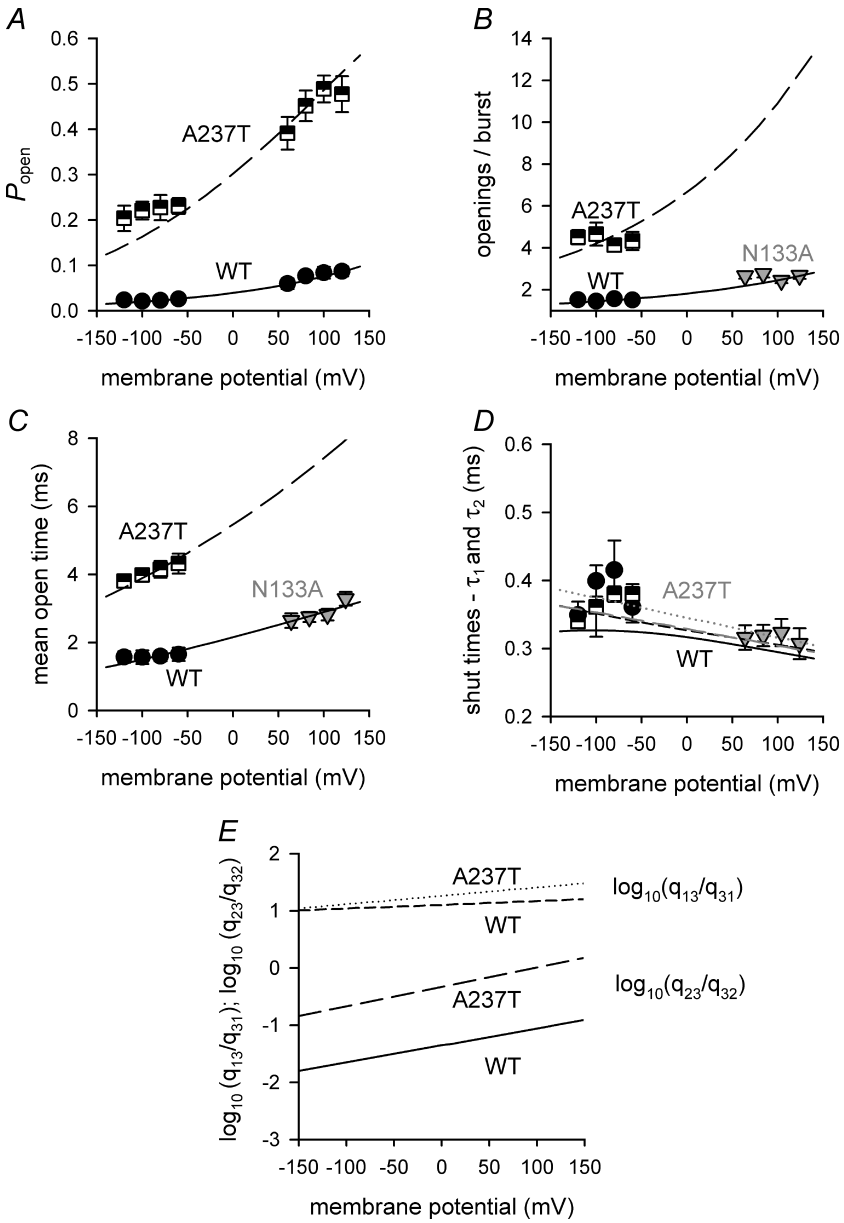

Figure 7. Modelling the gating kinetics of TASK-3 with a four-state model
A, relationship between P_{open} (ordinate) and membrane potential (abscissa) for the wild-type channel (WT) and the A237T mutant. Results are given as means ± S.E.M. and plotted for wild-type (filled circles) and A237T (semi-filled squares) at the voltage used in recording. The continuous line gives the predicted values for P_{open} in wild-type, using the four-state model – CO (state 1), OC (state 2), OO (state 3) and CC (state 4) – described by Scheme 1. Similarly, the dashed line indicates the predicted values for P_{open} in A237T, using the same four-state model. For wild-type, the estimated transition rate constants are given by the expressions: $q_{13} = 2.87\exp(0.000936V)$ ms^{-1}; $q_{31} = 0.226\exp(-0.000573V)$ ms^{-1}; $q_{23} = 0.0105\exp(0.00101V)$ ms^{-1} and $q_{32} = 0.238\exp(-0.00586V)$ ms^{-1}. For A237T the expressions are: $q_{13} = 2.87\exp(0.000928V)$ ms^{-1}, $q_{31} = 0.157\exp(-0.00245V)$ ms^{-1}; $q_{23} = 0.0122$ ms^{-1} and $q_{32} = 0.0260\exp(-0.00782V)$ ms^{-1}. The membrane potential V is given in mV. With A237T, the fit to the model predicted that q_{23} is independent of voltage. *B*, the continuous and dashed lines give the number of openings per burst (ordinate) for wild-type (WT) and A237T, respectively, as a function of membrane potential (abscissa) predicted from the four-state model. The data points for wild-type and A237T are represented as above in *A*. The data plotted for N133A (grey inverted triangles) were adjusted in their position along the abscissa by subtracting the shift in the Boltzmann relationship used in Results (eqn (3)) to fit the open state probability in these mutant channels. Similarly good fits were achieved for other mutants using a similar strategy (not shown). *C*, the continuous and dashed lines give the fit to mean open time (ordinate) for wild-type (WT) and A237T respectively, plotted against membrane potential (abscissa).

that seen in A237T ($P < 0.001$), but not significantly different from that in N133A ($P > 0.05$). The number of openings per burst at −120 mV was 2.66 ± 0.13 ($n = 5$)for N133A and 3.85 ± 0.77 for N133A/A237T. The value for N133A/A237T is significantly higher than that found for wild-type ($P < 0.01$), but is not significantly lower than that found for A237T.

Our use of the Boltzmann expression of eqn (3) suggests that the gating charge is not altered by mutation. We have tested this in a number of ways. First, we have fitted eqn (3) to the measurements for wild-type and for all mutants. Such a procedure gives a gating charge of 0.17 (with a standard deviation for the fit of 0.02) – the same value as that found for wild-type alone. Secondly, we show plots of $\ln P_{\text{open}}$ for mutants where P_{open} is sufficiently low that the values are still close to the foot of the relationship (Fig. 5*D*). Thirdly, we show P_{open} for all mutants plotted against $(V–V')$ as Supplemental Fig. 1. The hypothesis that gating charge is unaltered in the mutants we have made fits the results well.

Coupling energy. The effects of the two mutations (N133A and A237T) on the voltage dependence of P_{open} – on the value of V' in eqn (3) – would be expected to add in a simple way if the residues do not interact in any way (see for example, Carter *et al.* 1984; Horovitz, 1987; Hidalgo & MacKinnon, 1995). Thus, in the absence of an interaction,

$$\Delta G'_{\text{ww}} + \Delta G'_{\text{mm}} = \Delta G'_{\text{wm}} + \Delta G'_{\text{mw}}, \qquad (4)$$

where the subscripts w and m denote wild-type and mutant, respectively, for positions 133 and 237. $\Delta G'$ denotes the energy difference between open and shut forms of the channel computed from values of V'. The energy differences between open and shut forms are 7.5 kJ mol^{-1} ($\Delta G'_{ww}$) for wild-type and 3.4 kJ mol^{-1} ($\Delta G'_{\text{mm}}$) for the double mutant. The energy differences are 4.5 ($\Delta G'_{\text{mw}}$) and 2.1 kJ mol^{-1} ($\Delta G'_{\text{wm}}$), respectively, for the mutants N133A and A237T. Since the equality required by eqn (4) does not hold, these results give a coupling energy of 4.3 kJ mol^{-1}, consistent with an interaction between Thr in position 237 and Asn in position 133 in the mutant A237T. We believe the results are consistent with an H-bond contributing to the stabilising of the open state in A237T as predicted by the structural model (Fig. 5*C*). The strength of a hydrogen bond varies (for example with bond length, bond angle, and the polarity of the micro-environment; see for example Gao *et al.* 2009). Fersht *et al.* (1985) give the energy for H bonds between uncharged groups in the range 0.5–1.5 kcal mol^{-1} (2.1–6.3 kJ mol^{-1}). Since in the dimeric mutant channel two H-bonds would be formed to help stabilise the open state, our estimate of 4.3 kJ mol^{-1} is in the range given by Fersht *et al.* (1985) and our results are consistent with the hypothesis of the model of Fig. 5*C*.

Mutation of hinge glycines reduces P_{open}. To test further whether channels open and shut in the way envisaged in Fig. 5*C*, by flexion around hinge glycines, we have also made the relatively conservative mutations G117A in M2 and G231A in M4. Both mutants have a reduced P_{open}. Here the relationship between P_{open} and voltage was shifted to more positive voltages compared with wild-type channels (Fig. 5*B* and *D*), as anticipated from the gating hypothesis. In G231A, the mean open time was significantly reduced from that in wild-type to 0.75 ± 0.10 ms at −120 mV ($n = 7$; $P < 0.05$; see Fig. 5*E*). The number of openings per burst for G231A at −120 mV was 1.23 ± 0.04 ($n = 7$). The mutants favour the shut state and a larger depolarisation is required to open channels.

With the exception of A237T, in none of the mutants of M2 and M4 was the unitary conductance significantly altered from the value found in wild-type ($P > 0.05$ in each case). The values were: N133A, 21.9 ± 0.3 pS ($n = 5$); N133A/A237T, 20.1 ± 0.7 pS ($n = 7$); G117A, 15.4 ± 0.6 pS ($n = 5$); and G231A, 18.3 ± 1.4 pS ($n = 7$). Further, although mean open time (Fig. 5*E*) and number of openings per burst (not illustrated) were altered, in none of the mutants was the briefer population of shut times altered significantly in duration (see also Figs 2 and 4).

Mutants and the response to extracellular acidification

Talley & Bayliss (2002) have emphasised that in TASK-1, mutations that alter the responses to gating by receptors

Transition rates and data points for open time are as above in *A* and *B*. *D*, the continuous and dashed lines give the duration of two classes of brief closures (τ_1 and τ_2; ordinate) predicted by the four-state model for wild-type (WT) and for A237T respectively as functions of the membrane potential (abscissa). Again, transition rates and data points are as above. The duration of the two classes of brief closures are very similar for both the wild-type and A237T and would not be identified experimentally. For the wild-type channel, the predictions of the model for τ_1 are given as a continuous black line; those for τ_2 are shown as a short dashed black line. For A237T, the predictions for τ_1 are given as a long dashed grey line and for τ_2 as a dotted grey line. *E*, the equilibrium position of the two gating modes (*fast* and *slow*) are plotted as $\log_{10}(q_{13}/q_{31})$ and $\log_{10}(q_{23}/q_{32})$, respectively, against the membrane potential for wild-type (continuous and short-dashed lines) and for A237T (long-dashed and dotted lines) channel types. Voltage and mutations in membrane helices M2 and M4 affect principally the slower ($\log_{10}(q_{23}/q_{32})$) conformational change, owing to large change in q_{32}.

coupled to Gq or to volatile anaesthetics fail to alter the response to extracellular acidification. If the response to voltage involves a conformation change similar to that envisaged with Gαq or with halothane – opening and closing through flexion of M2 and M4 around hinge glycines – it is anticipated that the response to acidification will also be little altered in the mutants A237T, G117A and G231A. This expectation turns out to be correct.

Figure 6 shows the results of measurements of potassium currents recorded by two electrode voltage clamp in oocytes in different pH_o. Currents are plotted after being normalised to their value in pH 8.0. Since currents would be expected to be smaller in G117A and G231A, but larger in A237T, owing to differences in P_{open} at any given voltage, we injected 60- to 80-fold *more* cRNA into oocytes to obtain measurable current for mutants G117A and G231A and 2- to 3-fold *less* cRNA for A237T. In these three mutants, acidification reduces currents in G117A and G231A (Fig. 6*A* and *B*) and in A237T (Fig. 6*C*) much as it does in wild-type, with little apparent change in pK. The result for A237T corrects the account we have previously reported in abstract form, that A237T gives currents that are independent of changes of extracellular pH (Ashmole *et al.* 2005; Yuill *et al.* 2005). We have been unable to repeat that observation and have been unable to uncover the cause of our previous error.

Our results (Fig. 6) are in agreement with the expectation that gating in response to acidification does not involve gating at the cytoplasmic mouth of the channel.

Discussion

We have used both two electrode voltage clamp and single channel recording to investigate the response of TASK-3 channels to voltage. These channels have a very low P_{open} at negative voltages, but respond to depolarisation with an increase in this quantity. P_{open} increased 2.1-fold between −70 and +40 mV, as measured in 140 mM K_o^+ solutions (Fig. 3), similar to the 2.0-fold increase that occurred when external pH was increased from 6.0 to 7.0 (Fig. 6).

We show that the response to voltage occurs through opening and closing of the channel at its inner mouth, through movement of the inner membrane helices M2 and M4. Thus, mutants where residues close to this inner mouth are altered (A237T, N133A and N133A/A237T) stabilise the open state; mutants of hinge glycine residues (G117A and G231A) reduce the time spent open. The mutants shift the relationship between P_{open} and voltage: A237T and N133A to less positive voltages; G117A and G231A to more positive voltages. Mutants that alter side chain–side chain interactions in the region where gating occurs alter the stability of shut and open states. Our results, analysed using the theory of mutant cycles (Carter *et al.* 1984; Horovitz, 1987; Hidalgo & MacKinnon, 1995), indicate that in the mutant A237T, an H-bond contributes to stabilising the open state. Ben-Abu *et al*. (2009) have recently argued that the *Drosophila* channel KCNK0 – which, unlike TASK-3, has a high P_{open} in wild-type – remains open because of a lack of interaction among residues to stabilise the shut state of the cytoplasmic gate. This *Drosophila* channel is nevertheless shut by mutation of hinge glycine residues (Ben-Abu *et al.* 2009), as occurs here with TASK-3.

We do not have an explanation as to how the response to voltage is initiated. It occurs in the absence of any obvious voltage sensor, such as is found in Kv channels. In KcsA, voltage-dependent gating occurs in part at the selectivity filter and is driven by a charged residue (E71) in this filter (Cordero-Morales *et al.* 2006). No such charged residue is present in either TASK-1 or in TASK-3 and introducing a charge into the filter of TASK-1 did not alter the response to voltage (Yuill *et al.* 2007). Further, replacement in TASK-3 of certain charged residues elsewhere in the structure – in mutants K107Q, E130Q and R245Q – appears not to affect the response to voltage (data not shown). Nor does voltage sensing arise from the dipole moment of the helices that move to open the channel. These moving elements are the C-terminal parts of M2 and M4, lying on the cytoplasmic side of the hinge glycines G117 and G231. In each case, the negatively charged end of the dipole is at the cytoplasmic end (the C-terminal end) of the helices. If the helix dipole senses voltage field, the helices M2 and M4 would straighten under depolarisation, favouring the shut state. A possibility is that increasing occupancy by K^+ raises P_{open} and certainly the response to voltage is affected by the concentration of permeant ions (Lopes *et al.* 2000).

Whatever the mechanism that initiates the response to voltage, there are striking parallels between this response and the response of K_{2P} channels to Gq coupled receptors (Millar *et al.* 2000; Czirják *et al.* 2000; Talley *et al.* 2000) and to volatile anaesthetics (Talley & Bayliss, 2002). The response to halothane is regulated by residues in M2 and M4, close to the cytoplasmic mouth, both in a TASK homologue in *Lymnaea* (Andres-Enguix *et al.* 2007) and in TASK-1 (Talley & Bayliss, 2002). The region is also involved in down-regulation of channels by Gq coupled pathways (Talley & Bayliss, 2002; Veale *et al.* 2007). The response to both Gαq and halothane (Talley & Bayliss, 2002) and the response to voltage (this paper) occur apparently independently of the response to acidification.

Kinetic modelling of TASK-3. We have used our experimental results to develop a minimal, physiologically plausible kinetic model of TASK-3. The model includes two mutually independent gates in either an open (O) or close state (C), thus generating a channel state-diagram

with one open (OO) and three shut (CC, CO, OC) states (Scheme 1). We have in mind that one of these

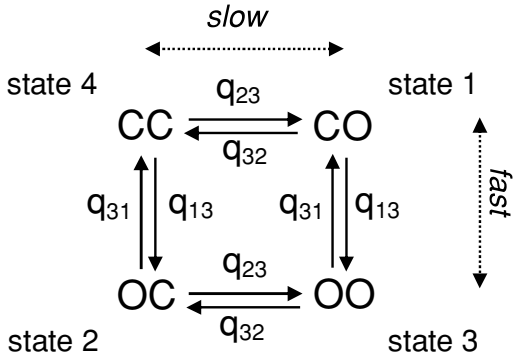

Scheme 1

gates will be associated principally with the selectivity filter of the channel and the other with its cytoplasmic mouth. Shutting of each gate results either in a slow (OC→OO/CC→CO) or in a fast (CO→OO/CC→OC) state transition, which we shall refer to as the 'two modes of gating' of the channel.

Some results from fitting the model of Scheme 1 against data from wild-type and A237T mutant channels (see Methods) are given in Fig. 7. In formulating the model, we have used P_{open} (Fig. 7*A*), number of openings per burst (Fig. 7*B*), mean open time (Fig. 7*C*) and mean duration of brief closures (Fig. 7*D*). Since we have relatively little information from single channel patches in wild-type at positive membrane potentials, we have also used information from recordings from N133A to augment these data (see legend to Fig. 7).

The model fits well the single channel data in both the wild-type (WT; continuous lines) and A237T (dashed lines) channels (Fig. 7*A*–*D*), indicating that a minimal kinetic mechanism incorporating two types of conformational change (presumably corresponding to opening and shutting at the selectivity filter and at the cytoplasmic mouth of the channel) is sufficient to explain important aspects of single-channel activity in wild and mutant types. However, the model underestimates the duration of long closures in wild-type by 65% and overestimates the duration in A237T by 80%, both at −120 mV (data not shown).

Naturally, a four state model predicts two classes of brief closures (τ_1 and τ_2; Fig. 7*D*), instead of the single class found experimentally (Figs 2 and 4). However, since their lifetimes are virtually identical, these two classes of brief closures would not be discriminated in single channel recording.

Figure 7*E* shows the equilibrium position for the two modes of gating of the channel, represented as q_{13}/q_{31} (fast) and q_{23}/q_{32} (slow) for wild-type and A237T. The slower gating process (q_{23}/q_{32}) is the one more affected by voltage and by mutation, with mutation affecting principally the transition rate constant q_{32}, which determines entry into the long lived shut state.

References

Andres-Enguix I, Caley A, Yustos R, Schumacher MA, Spanu PD, Dickinson R, Maze M & Franks NP (2007). Determinants of the anaesthetic sensitivity of two-pore domain acid-sensitive potassium channels: molecular cloning of an anaesthetic-activated potassium channel from *Lymnaea stagnalis*. *J Biol Chem* **282**, 20977–20990.

Ashmole I, Goodwin PA & Stanfield PR (2001). TASK-5, a novel member of the tandem pore K^+ channel family. *Pflugers Arch* **442**, 828–833.

Ashmole I, Yuill K & Stanfield P (2005). Mutation of the alanine residue A237 abolishes sensitivity of the tandem pore K^+ channel TASK-1 to extracellular pH. *J Physiol* **557.P**, PC84.

Ben-Abu Y, Zhou Y, Zilberbeg N & Yifrach O (2009). Inverse coupling in leak and voltage activated K^+ channel gates underlies distinct roles in electrical signalling. *Nat Struct Mol Biol* **16**, 71–79.

Bichet D, Haass FA & Jan LY (2003). Merging functional studies with structures of inward-rectifier K^+ channels. *Nat Rev Neurosci* **4**, 957–967.

Boeckmann B, Bairoch A, Apweiler R, Blatter MC, Estreicher A, Gasteiger E, Martin MJ, Michoud K, O'Donovan C, Phan I, Pilbout S & Schneider M (2003). The SWISS-PROT protein knowledgebase and its supplement TrEMBL in 2003. *Nucleic Acids Res* **31**, 365–370.

Brickley SG, Aller MI, Sandu C, Veale EL, Alder FG, Sambi H, Mathie A & Wisden W (2007). TASK-3 two-pore domain potassium channels enable sustained high-frequency firing in cerebellar granule neurons. *J Neurosci* **27**, 9329–9340.

Carter PJ, Winter G, Wilkinson AJ & Fersht AR (1984). The use of double mutants to detect structural changes in the active site of the tyrosyl-tRNA sythetase (*Bacillus stearothermophilus*). *Cell* **38**, 835–840.

Chemin J, Girard C, Duprat F, Lesage F, Romey G & Lazdunski M (2003). Mechanisms underlying excitatory effects of group I metabotropic glutamate receptors via inhibition of 2P domain K^+ channels. *EMBO J* **22**, 5403–5411.

Colquhoun D & Hawkes AG (1995). A Q-matrix cookbook. In *Single Channel Recording*, ed. Sakmann B & Neher E, pp. 589–633. Plenum, New York.

Colquhoun D & Sakmann B (1985). Fast events in single-channel currents activated by acetylcholine and its analogues at the frog muscle end-plate. *J Physiol* **369**, 501–557.

Colquhoun D & Sigworth FJ (1995). Fitting and statistical analysis of single-channel records. In *Single Channel Recording*, ed. Sakmann B & Neher E, pp. 483–587. Plenum, New York.

Cordero-Morales JF, Cuello LG & Perozo E (2006). Voltage dependent gating at the KcsA selectivity filter. *Nat Struct Mol Biol* **13**, 319–322.

Czirják G & Enyedi P (2002). TASK-3 dominates the background potassium conductance in rat adrenal glomerulosa cells. *Mol Endocrinol* **16**, 621–629.

Czirják G, Fischer T, Spät A, Lesage F & Enyedi P (2000). TASK (TWIK-related acid-sensitive K^+ channel) is expressed in glomerulosa cells of rat adrenal cortex and inhibited by angiotensin II. *Mol Endocrinol* **14**, 863–874.

de la Cruz IP, Levin JZ, Cummins C, Anderson P & Horvitz HR (2003). *sup*-9, *sup*-10, and *unc*-93 may encode components of a two-pore K^+ channel that coordinates muscle contraction in *Caenorhabditis elegans*. *J Neurosci* **23**, 9133–9145.

Doyle DA, Morais Cabral J, Pfuetzner RA, Kuo A, Gulbuis JM, Cohen SL, Chait BT & MacKinnon R (1998). The structure of the potassium channel: molecular basis of K^+ conduction and selectivity. *Science* **280**, 69–77.

Duprat F, Lesage F, Fink M, Reyes R, Heurteaux C & Lazdunski M (1997). TASK, a human background K^+ channel to sense external pH variations near physiological pH. *EMBO J* **16**, 5464–5471.

Fanjul M & Hollande E (1993). Morphogenesis of 'duct-like' structures in three-dimensional cultures of human cancerous pancreatic duct cells (Capan-1). *In Vitro Cell Dev Biol Anim* **29A**, 574–584

Fersht AR, Shi J-P, Knill-Jones J, Lowe DM, Wilkinson AJ, Blow DM, Brick P, Carter P, Waye MMY & Winter G (1985). Hydrogen bonding and biological specificity analysed by protein engineering. *Nature* **314**, 235–238.

Gao J, Bosco DA, Powers ET & Kelly JW (2009). Localized thermodynamic coupling between hydrogen bonding and microenvironment polarity substantially stabilizes proteins. *Nat Struct Mol Biol* **16**, 684–691.

Goldstein SA, Bockenhauer D, O'Kelly I & Zilberberg N (2001). Potassium leak channels and the KCNK family of two-P-domain subunits. *Nat Rev Neurosci* **2**, 175–184

Han J, Truell J, Gnatenco C & Kim D (2002). Characterization of four types of background potassium channels in rat cerebellar granule neurons. *J Physiol* **542**, 431–444.

Han J, Gnatenco C, Sladek CD & Kim D (2003). Background and tandem-pore potassium channels in magnocellular neurosecretory cells of the rat supraoptic nucleus. *J Physiol* **546**, 625–639.

Hidalgo P & MacKinnon R (1995). Revealing the architecture of a K^+ channel pore through mutant cycles with a peptide inhibitor. *Science* **268**, 307–310.

Horovitz A (1987). Non-additivity in protein-protein interactions. *J Mol Bio* **196**, 733–735.

Jiang Y, Lee A, Chen J, Cadene M, Chait BT & MacKinnon R (2002). Crystal structure and mechanism of a calcium-gated potassium channel. *Nature* **417**, 515–522.

Jiang Y, Lee A, Chen J, Ruta V, Cadene M, Chait BT & MacKinnon R (2003). X-ray structure of a voltage-dependent K^+ channel. *Nature* **423**, 33–41.

Kim D, Fujita A, Horio Y & Kurachi Y (1998). Cloning and functional expression of a novel cardiac two-pore background K^+ channel (cTBAK-1). *Circ Res* **82**, 513–518.

Kim D (2005). Physiology and pharmacology of two-pore domain potassium channels. *Curr Pharm Des* **11**, 2717–2736.

Kim Y, Bang H & Kim D (2000). TASK-3 a novel member of the tandem pore K^+ channel family. *J Biol Chem* **275**, 9340–9347.

Kuo A, Gulbis JM, Antcliff JF, Rahman T, Lowe ED, Zimmer J, Cuthbertson J, Ashcroft FM, Ezaki T & Doyle DA (2003). Crystal structure of the potassium channel KirBac1.1 in the closed state. *Science* **300**, 1922–1926.

Leonoudakis D, Gray AT, Winegar BD, Kindler CH, Harada M, Taylor DM, Chavez RA, Forsayeth JR & Yost CS (1998). An open rectifier potassium channel with two pore domains in tandem cloned from rat cerebellum. *J Neurosci* **18**, 868–877.

Lopes CMB, Gallagher PG, Buck ME, Butler MH & Goldstein SAN (2000). Proton block and voltage gating are potassium dependent in the cardiac leak channel Kcnk3. *J Biol Chem* **275**, 16969–16978.

Lopes CMB, Zilberberg N & Goldstein SAN (2001). Block of Kcnk3 by protons. *J Biol Chem* **276**, 24449–24452.

Lopes CM, Rohács T, Czirják G, Balla T, Enyedi P & Logothetis DE (2005). PIP_2 hydrolysis underlies agonist-induced inhibition and regulates voltage gating of two-pore domain K^+ channels. *J Physiol* **564**, 117–129.

Millar JA, Barratt L, Southan AP, Page KM, Fyffe RE, Robertson B & Mathie A (2000). A functional role for the two-pore domain potassium channel TASK-1 in cerebellar granule neurons. *Proc Natl Acad Sci U S A* **97**, 3614–3618.

Morton MJ, O'Connell AD, Sivaprasadarao A & Hunter M (2003). Determinants of pH sensing in the two-pore domain K^+ channels TASK-1 and -2. *Pflugers Arch* **445**, 557–583.

Patel AJ & Honoré E (2001). Properties and modulation of mammalian 2P domain K^+ channels. *Trends Neurosci* **24**, 339–346.

Rajan S, Wischmeyer E, Xin Liu G, Preisig-Muller R, Daut J, Karschin A & Derst C (2000). TASK-3, a novel tandem pore domain acid-sensitive K^+ channel. An extracellular histidine as pH sensor. *J Biol Chem* **275**, 16650–16657.

Sigworth FJ & Sine SM (1987). Data transformations for improved display and fitting of single-channel dwell time histograms. *Biophys J* **52**, 1047–1054.

Stanfield PR, Ashmole I, Stansfeld PJ & Sutcliffe MJ (2008). TASK-3 potassium channels: gating at the cytoplasmic mouth of the channel. *Proc Physiol Soc* **11**, C41.

Stansfeld PJ, Grottesi A, Sands ZA, Sansom MS, Gedeck P, Gosling M, Cox B, Stanfield PR, Mitcheson JS & Sutcliffe MJ (2008). Insight into the mechanisms of inactivation and pH sensitivity in potassium channels from molecular dynamics simulations. *Biochemistry* **47**, 7414–7422.

Talley EM, Lei Q, Sirois JE & Bayliss DA (2000). TASK-1, a two pore domain K^+ channel, is modulated by multiple neurotransmitters in motoneurons. *Neuron* **25**, 399–410.

Talley EM & Bayliss DA (2002). Modulation of TASK-1 (Kcnk3) and TASK-3 (Kcnk9) potassium channels: volatile anaesthetics and neurotransmitters share a molecular site of action. *J Biol Chem* **277**, 17733–17742.

Veale EL, Buswell R, Clarke CE & Mathie A (2007). Identification of a region in the TASK3 two pore domain potassium channel that is critical for its blockade by methanandamide. *Br J Pharmacol* **152**, 778–786.

Washburn CP, Sirois JE, Talley EM, Guyenet PG & Bayliss DA (2002). Serotonergic raphe neurons express TASK channel transcripts and a TASK-like pH- and halothane-sensitive K^+ conductance. *J Neurosci* **22**, 1256–1265.

Yellen G (1998). The moving parts of voltage-gated ion channels. *Q Rev Biophys* **31**, 239–295.

Yuill KH, Ashmole I & Stanfield PR (2005). The acid sensitive K^+ channel TASK-1: mutation of the residue A237 abolishes sensitivity to extracellular pH. 2005 Biophysical Society Meeting Abstracts. *Biophys J* Supplement 2320 Pos.

Yuill KH, Stansfeld PJ, Ashmole I, Sutcliffe MJ & Stanfield PR (2007). The selectivity, voltage-dependence and acid sensitivity of the tandem pore potassium channel TASK-1: contributions of the pore domains. *Pflugers Arch* **455**, 333–348.

Zilberberg N, Ilan N & Goldstein SAN (2001). KCNK0: opening and closing the 2-P domain potassium leak channel entails 'C-type' gating of the outer pore. *Neuron* **32**, 635–648.

Author contributions

All authors contributed to the conception, design, analysis and/or interpretation of the data presented in this paper. The electrophysiological experiments were designed by PRS and IA and carried out principally by IA, who also designed and carried out the molecular biological procedures. Analysis of the electrophysiological experiments was done by PRS. Some preliminary analysis was carried out by PRM, who also contributed to cell culture and transfection procedures. The structural modelling was carried out by PJS and MJS. The kinetic modelling was done by DVV and JFF. The paper was written by PRS, initially in collaboration with IA and DVV, and revised with the critical appraisal of PJS, JFF and MJS. The substantive contributions to experiment and modelling were made by IA, DVV, and PJS. All authors approved the final version of the paper for publication.

Acknowledgements

We thank the Wellcome Trust for support. D.V.V. was supported by the EU-funded project BION. We also thank Professor R. B. Freedman for help with mutant cycles.